



Dynamics, Chaos and Synchronization of Self-sustained Electromechanical Systems with Clamped-free Flexible ARM

C.A. KITIO KWUIMY & P. WOAFO

An electromechanical system with flexible arm is considered. The mechanical part is linear flexible beam and the electrical part is nonlinear self sustained oscillator. Oscillatory solutions are obtained using averaging method. Chaotic behaviour is studied via the Lyapunov exponent. The synchronization of regular and chaotic states of two such devices is discussed and the stability boundaries for the synchronization process are derived using the Floquet theory. We compare the results the results obtained from a finite difference simulation to those from the classical modal approach.

Keywords: Electromechanical devices, flexible arms, oscillatory and chaotic states, synchronization.

1. INTRODUCTION

Recently various studies have been devoted to nonlinear electromechanical devices consisting of a nonlinear electric circuit coupled magnetically electrostatically to rigid arm [1-7]. These devices are described by two coupled nonlinear differential equations. The particular interest to these devices is that they are inherently present in everyday life both at the domestic and industrial levels for the automation of various processes [2]. This is for example the case of multi-frequency or chaotic industrial shaker.

The aim of this paper is to extend the above studies to electromechanical devices with flexible arms. This constitutes a new mathematical and numerical challenge. Moreover, this is a new interesting area of application since many industrial tasks are carried out through flexible structures. The device under consideration here consists of a Rayleigh-Duffing electrical circuit coupled magnetically to a clamped-free flexible beam.

The paper is organized as follows. Section 2 consists of three parts. The first part presents the nonlinear electromechanical devices as well as the resulting partial differential equations. The second part considers the non-mode approximation of the beam dynamics to derive a set

of two nonlinear differential equations for the amplitudes of the first mode and electric charge of the capacitor. These equations constitute the basis of the analytical and the semi-analytical investigation. The third part of section 2 deals with the presentation of the finite difference algorithm for the direct numerical simulation of the full equations of the electromechanical device. In section 3, the averaging method is used to derive approximate oscillatory states whose amplitudes are compared to the results of the numerical simulation. Section 4 is devoted to the question of chaotic behaviour while section 5 uses the unidirectional coupling scheme to find the good parameters leading to the synchronization of a second similar device (slave device) to the motion of the first device called master. This is done both in the case of periodic oscillatory and chaotic behavior. Conclusion is given in section 6.

2. MODEL, EQUATIONS AND NUMERICAL SCHEME

2.1 Model

The model shown in Figure 1 is an electrical oscillator coupled through a magnet to a clamped-free flexible beam. The electrical part consists of a non-linear resistor (NLR), a non linear condenser (NLC) C and an inductor L , all connected in series. Two types of non linear components are considered in the model. The voltage of the condenser is a non linear function of the instantaneous electrical charge and is expressed by

$$V_C = \frac{1}{C_0} q_0 + a_3 q_0^3 \quad (1)$$

where C_0 is the linear value of C and a_3 is a non linear coefficient depending on the type of the capacitor [8]. The current- voltage characteristics of the resistor is defined as

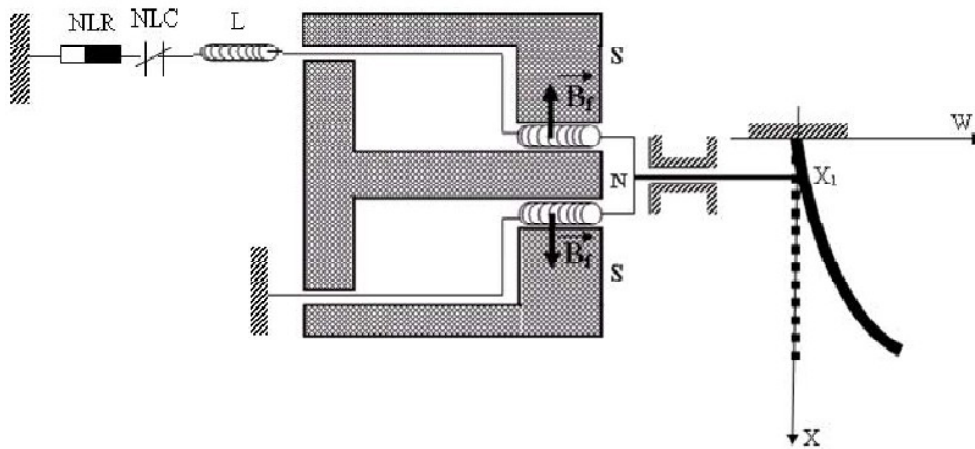


Figure 1: An electromechanical transducer with clamped-free flexible arm

$$V_R = -R_0 i_0 \left(\frac{i}{i_0} - \frac{1}{3} \left(\frac{i}{i_0} \right)^3 \right) \quad (2)$$

where R_0 and i_0 are, respectively, the characteristics resistance and current; i is the current through the resistor. This non linear resistor can be realized using a block consisting of two transistors [9] or series of diodes [10]. With this resistor the system has the property to exhibit self excited oscillations. The current-voltage characteristics of the linear inductor is

$$V_L = L \frac{di}{d\tau} \quad (3)$$

where τ is the time.

The mechanical part is a flexible beam of length l_0 . The beam is presumed to be a slender, isotropic, uniform rod. It is fixed at its top and free at the base. The magnetic coupling between both parts is made at a point X_1 . It creates the Laplace force in the mechanical part and the Lenz electromotive voltage in the electrical part. Using the electrical and mechanical laws, it is found that the model is described by the following equations

$$L \frac{d^2 q_0}{d\tau^2} - R_0 \left(1 - \frac{1}{3i_0^2} \left(\frac{dq_0}{d\tau} \right)^2 \right) \frac{dq_0}{d\tau} + \frac{q_0}{C_0} + a_3 q_0^3 = -B_f l \frac{\partial W}{\partial \tau} \delta(X - X_1) \quad (4)$$

$$\rho S \frac{\partial^2 W}{\partial \tau^2} + \lambda \frac{\partial W}{\partial \tau} + EI \frac{\partial^4 W}{\partial X^4} = \frac{B_f l}{l_0} \frac{dq_0}{d\tau} \delta(X - X_1). \quad (5)$$

The beam boundary conditions are given as follows

$$W(0, \tau) = 0; \left(\frac{\partial W}{\partial X} \right) (0, \tau) = 0, \quad \forall \tau \in \mathbb{R}_+, \quad \text{at the clamped end,} \quad (6)$$

$$\left(\frac{\partial^2 W}{\partial X^2} \right) (l_0, \tau) = 0, \quad \left(\frac{\partial^3 W}{\partial X^3} \right) (l_0, \tau) = 0, \quad \forall \tau \in \mathbb{R}_+ \quad \text{at the free end.} \quad (7)$$

E is the Young modulus of the beam, ρ is the beam density, S and I are respectively the area and the moment of inertial of the beam cross section. $W(X, \tau)$ is the transversal deflection of the beam, X is the spatial coordinate, λ is the mechanical damping coefficient which is

assumed to be constant, B_f is the intensity of the magnetic field and l is the length of the current wire in the coupling domina. $\delta(\cdot)$ stands for the Dirac delta function, it expresses the fact that the coupling is made at a point X_1 of the flexible beam.]

We introduceteh dimensionless variables

$$t = \omega_1 \tau, \quad v = \frac{W}{l_0}, \quad x = \frac{X}{l_0}, \quad q_0 = Qq, \quad (8)$$

Where $\omega_1 = (1.875)^2 \text{ rad/s}$ and $Q = \frac{i_0}{\omega_0} \sqrt{3}$. Consequently, equations (4) and (5) become

$$\frac{d^2 q}{dt^2} - \varepsilon_1 \left(1 - \left(\frac{dq}{dt} \right)^2 \right) \frac{dq}{dt} + w_0^2 q + bq^3 = -f_2 \frac{\partial v}{\partial t} \delta(x - x_1) \quad (9)$$

$$\frac{\partial^2 v}{\partial t^2} + \varepsilon_2 \frac{\partial v}{\partial t} a^2 \frac{\partial^4 v}{\partial x^4} = f_1 \frac{dq}{dt} \delta(x - x_1), \quad (10)$$

with

$$\varepsilon_1 = \frac{R_0}{L\omega_1}, \quad \omega_0^2 = \frac{1}{LC_0\omega_1^2}, \quad b = \frac{a_3 Q^2}{L\omega l^2}, \quad f_2 = \frac{B_f l_0 l}{L\omega_1 Q},$$

$$\varepsilon_2 = \frac{\lambda}{\rho S \omega_1}, \quad a^2 = \frac{EI}{\rho S l_0^4 \omega_1^2}, \quad f_1 = \frac{B_f l l_0}{L\omega_1 Q}.$$

and the boundary conditions (6) and (7) become

$$v(0, t) = 0, \quad \frac{\partial v}{\partial x}(0, t) = 0, \quad \forall \tau \in \mathbb{R}_+, \quad \text{at the clamped end,} \quad (11)$$

$$\frac{\partial^2 v}{\partial x^2}(1, t) = 0, \quad \frac{\partial^3 v}{\partial x^3}(1, t) = 0, \quad \forall \tau \in \mathbb{R}_+, \quad \text{at the free end.} \quad (12)$$

2.2 Mode Equations

For the analytical investigation, it is convenient to assume an expansion of the deflection $v(x, t)$ in terms of the combination of linear free oscillation. Due to the complexity of the

eigen-functions of the beam fixed at one end and free at the other, we will consider in the analytical treatment only the first mode. Thus we can write

$$v(x, t) = y_1(t) \phi_1(x) \quad (13)$$

where

$$\phi_1(x) \cos(k_1 x) - \cosh(k_1 x) - \frac{\cos(k_1) + \cosh(k_1)}{\sin(k_1) + \sinh(k_1)} [\sin(k_1 x) - \sinh(k_1 x)] \quad (14)$$

The expression of $\phi_1(x)$ can be found in classic books on beam dynamics such as Ref. [11]. The eigenvalue k_m for the mode m is obtained from the transcendental equation

$$\cos(k_m) \cosh(k_m) + 1 = 0 \quad (15)$$

This equation gives $k_1 \approx 1.875$.

Inerting equation (13) into equations (9) and (10), multiplying equation (10) by $\phi_1(x)$, intergrating over the non-dimensional length of the beam and using the orthogonality of eigenfunctions, we obtain

$$\frac{d^2 q}{dt^2} - \varepsilon_1 \left(1 - \left(\frac{dq}{dt} \right)^2 \right) \frac{dq}{dt} + w_0^2 q + bq^3 = -f_{21} \frac{dy_1}{dt} \quad (16)$$

$$\frac{d^2 y_1}{dt^2} + \varepsilon_2 \frac{dy_1}{dt} + w_0^2 y_1 = f_{11} \frac{dq}{dt} \quad (17)$$

$$f_{11} = f_1 \phi_1(x_1), \quad f_{21} = f_2 \phi_1(x_1) \quad \text{and} \quad w_{01}^2 = w_1^2 a^2$$

Thus the one-mode dynamics is described by a Rayleigh-Duffing oscillator coupled to a linear harmonic oscillator equaton. A linear stability analysis of the fixed stationary point

($q = 0, \frac{dq}{dt} = 0, y_1 = 0, \frac{dy_1}{dt} = 0$) shows that it is stable for $\varepsilon_1 < \varepsilon_2 < \frac{f_{11} f_{21}}{\varepsilon_1}$.

2.3 The Finite Difference Algorithm

For obtaining a numerical solution of equations (9) and (10), we use the finite difference scheme. In this respect, we divide the non-dimensional beam length in n intervals of length h_x , e.g. $h_x = \frac{1}{n}$. Also the time is discretized in units of length h_t . Therefore one can write $x_i = (i - 1) h_x$ and $t_j = j h_t$ where i and j are integer variables. Consequently, equations (9) and (10) become

$$\frac{d^2q}{dt} - \varepsilon_1 \frac{dq}{dt} \left(1 - \left(\frac{dq}{dt} \right)^2 \right) + w_0^2 q + bq^3 = -f_2 \frac{v_{i,j+1} - v_{i,j}}{h_t} \delta_{i-1,i_{x1}} \quad (18)$$

$$A_1 v_{i,j+1} + A_2 v_{i,j} + A_3 v_{i,j-1} + A_4 (v_{i+2,j} + v_{i-2,j}) + A_5 (v_{i+1,j} + v_{i-1,j}) = f_1 \frac{dq}{dt} \delta_{i-1,i_{x1}} \quad (19)$$

for $i = 2, \dots, n+1$ and $\forall j \in N$,

with

$$A_1 = \frac{1}{h_t^2} + \frac{\varepsilon_2}{2h_t}, A_2 = \frac{-2}{h_t^2} + \frac{6a}{h_t^4}, A_3 = \frac{1}{h_t^2} - \frac{\varepsilon_2}{2h_t}, A_4 = \frac{a^2}{h_x^4}, A_5 = 4A_4$$

$$v_{1,j} = 0, v_{0,j} = v_{2,j} \text{ at the clamped end,} \quad (20)$$

$$v_{n+2,j} = 2v_{n+1,j} - v_{n,j}, v_{n+3,j} = v_{n-1,j} + 2v_{n+2,j} - 2v_{n,j}, \text{ at the free end.} \quad (21)$$

One can show that the discretization scheme is stable is stable if

$$\frac{8}{h_x^4} \leq \frac{1}{h_t^2} \left[1 + \sqrt{1 - \frac{(\varepsilon_2 h_t)^2}{4}} \right] \quad (22)$$

with $\varepsilon_2 h_t \leq 2$

3. OSCILLATORY STATES

Oscillatory solutions of equations (11) and (12) are obtained by using the Krylov-Bogoliubov averaging method described in References [12,13]. In this line we set $q = A \sin(\omega_0 t + \varphi_1)$, $y_1 = B \sin(\omega_{01} t + \phi_2)$. The amplitudes A and B satisfy the following set of first order differential equations

$$\frac{dA}{dt} = \frac{\varepsilon_1 A}{2} \left(1 - \frac{3}{4} A^2 w_0^2 \right) - \frac{f_{21} B w_{01}}{2w_0} \cos(\varphi) \quad (23)$$

$$\frac{dB}{dt} = -\frac{\varepsilon_2 B}{2} + \frac{f_{11} A w_0}{2w_{01}} \cos(\varphi) \quad (24)$$

$$\frac{d\varphi}{dt} = \frac{3bA^2}{8w_0} + \left[\frac{f_{21} B w_{01}}{2A w_0} - \frac{f_{11} A w_0}{2B w_{01}} \right] \sin(\varphi) \quad (25)$$

with $\varphi = \varphi_1 - \varphi_2$. For the steady-states solutions, se obtain

$$c_6 A^6 + c_4 A^4 + c_2 A^2 + c_0 = 0 \quad (26)$$

$$B^2 = MA^2(4 - 3A^2 w_0^2) \quad (27)$$

$$c_6 = 27\mu v^2 w_0^6 + 3\chi w_0^2, \quad c_4 = 18\chi v w_0^4(1 - 4\eta) - 4\chi + 9v^2 w_0^4(1 - 4\mu),$$

$$c_2 = 6v w_0^2(1 - 4v)(1 - 4\mu) + 3\mu w_0^2(1 - 4v)^2,$$

$$c_0 = (1 - 4\mu)(1 - 4v^2), \quad v = \frac{\varepsilon_1}{4\varepsilon_2}, \quad \mu = \frac{\varepsilon_1 \varepsilon_2}{4f_{1n} f_{2n}},$$

$$k = \frac{\varepsilon_1}{\varepsilon_2 f_{1n} f_{2n} w_0^2}, \quad \chi = \frac{9b^2 k}{64}, \quad M = \frac{\varepsilon_1 w_0^2 f_{11}}{4\varepsilon_2 w_{0n}^2 f_{21}}. \quad (28)$$

Let us note that there is a trivial steady-state defined by $A_0 = B_0 = 0$. Equations (26) and (27) are solved using the Newton-Raphson algorithm.

Figures 2 and 3 show the amplitude curves of the beam at its free end and the charge of condenser in term of the mechanical dissipative coefficient ε_2 for two different sets of values of parameters of the system. The numerical simulation results of equations (16) and (17) those of equations (18) and (19) are also reported in the same figures. The numerical results of the equations (16) and (17) are called semi-analytical ones. For Figure 2, the analytical and semi-analytical curves show a complete quenching phenomena of oscillation in the region $\varepsilon_1 < \varepsilon_2 < \frac{f_{11} f_{21}}{\varepsilon_1}$. This results was also obtained in Refs. [1, 5] for a self-sustained oscillator coupled to a rigid rod. With this choice of values, the numerical curves (those from equations (18) and (19) do not corroborate this result. This is due to the fact that for the analytical and semi-analytical treatment, only one mode (the first) was taking into account. We observe that the effects of other modes, in spite of the fact that we are at the perfect resonance, can not be always neglected. Making another choice of values of the parameters, we obtain quenching phenomena also with the partial differential equation (Figure 3) for $0.032 < \varepsilon_2 < 0.53$, while with the semi-analytical treatment, this occurs for $0.01 < \varepsilon_2 < 0.73$. This corresponds to the stability interval $\varepsilon_1 < \varepsilon_2 < \frac{f_{11}}{f_{21}}$ of the statinary point ($q = 0, \frac{dq}{dt} = 0, y_1 = 0, \frac{dy_1}{dt} = 0$).

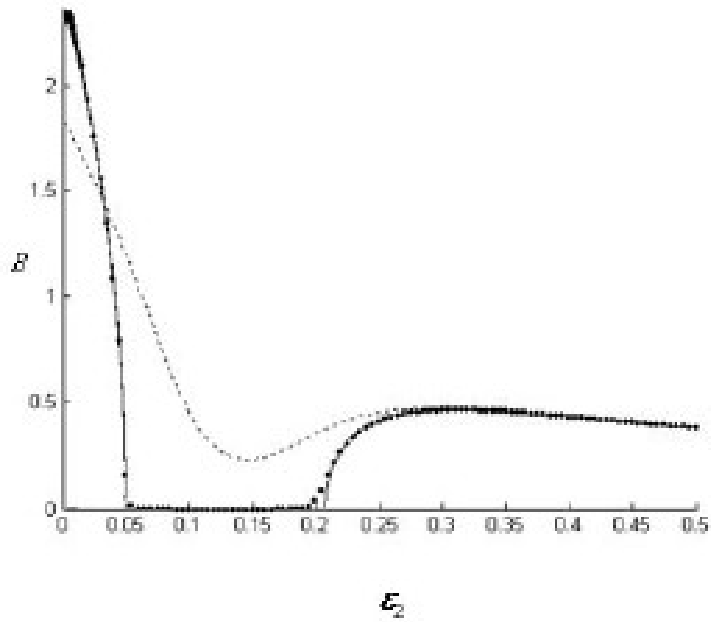


Figure 2a

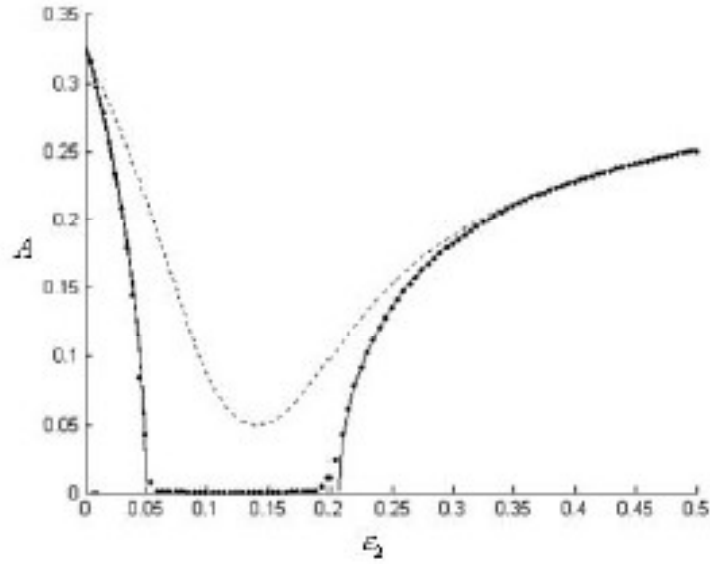


Figure 2b

Figure 2: Amplitudes of the mechanical part (a) and electrical part (b) as function of beam dissipation coefficient. Analytical curve (lines); semi-analytical curve (options); numerical curve (dash lines) with $b = 0.1$, $a = 1$, $w_{01} = w_0 = w_1 a$, $\epsilon_1 = 0.05$, $f_1 = 1.4$, $f_2 = 0.1$

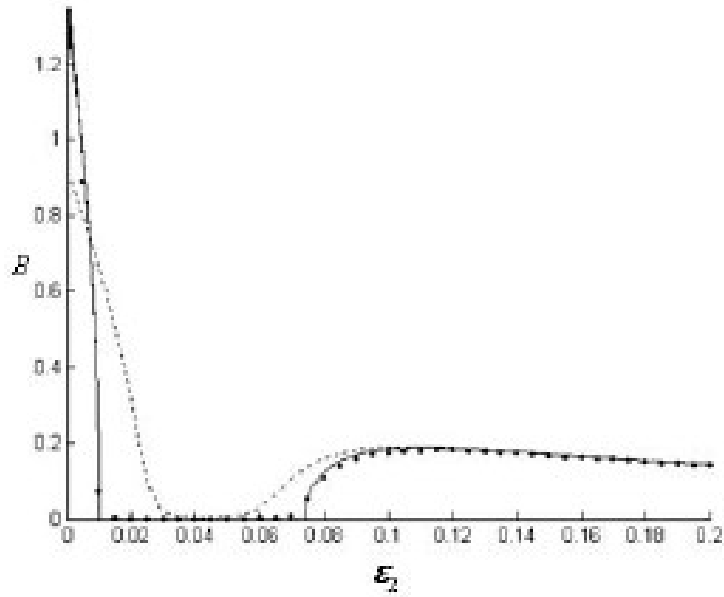


Figure 3a

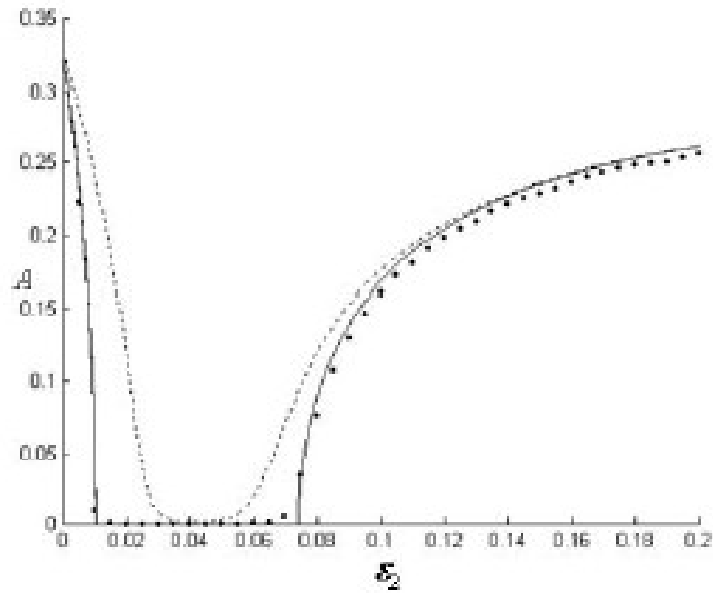


Figure 3b

Figure 3: Amplitudes of the mechanical part (a) and electrical part (b) as function of beam dissipation coefficient. Analytical curve (lines); semi-analytical curve (points); numerical curve (dash lines) with $b = 0.01$; $a = 1$; $w_{01} = w_0 = w_1 a$; $\varepsilon_1 = 0.01$; $f_1 = 0.2$; $f_2 = 0.05$

4. CHAOTIC BEHAVIOUR

In this section, we find how chaos arises in our device as its parameters evolve and compare the results of the modal approach to those of the direct numerical simulation of the partial differential equations. For this aim, we use the Lyapunov exponent. The results hereafter are obtained by numerically solving equations (16) and (17) and equations (18) and (19) with their corresponding variational equations. In the case of finite difference simulation, the Lyapunov exponent is defined by

$$lyan = \lim_{t \rightarrow \infty} \frac{\ln(d_1(t))}{t} \quad (29)$$

with

$$d_1 = \sqrt{dq^2 + \left(\frac{d}{dt}dq\right)^2 + \sum_{i=1}^n dv_i^2 + \sum_{i=1}^n \left(\frac{\partial}{\partial t}dv_i\right)^2} \quad (30)$$

while for the ordinary differential equation (equations (16) and (17)), one has

$$lyas = \lim_{t \rightarrow \infty} \frac{\ln(d_2(t))}{t} \quad (31)$$

with

$$d_2 = \sqrt{dq^2 + \left(\frac{d}{dt}dq\right)^2 + dy_1^2 + \left(\frac{d}{dt}dy_1\right)^2} \quad (32)$$

where dq , dv_i and dy_1 are the variation of q , v_i and y_1 respectively.

Figure 4 shows the Lyapunov exponent as the coupling coefficient f_2 increases. On finds that for $f_2 \in [1.85; 2.3]$ there is a series of domain corresponding to a chaotic dyanmics with the modal approach while with the finite difference scheme this occurs for $f_2 \in [1.6; 2.08] \cup [2.12; 2.25]$. For the two approaches we have plotted the phase portrait for a value of f_2 leading to chaos (see Figures 5 and 6). The results of Figures 4 to 6 show an almost qualitative agreement between the modal approach and the finite difference simulation. However, one finds that the chaotic domains predicted by the first approach are different to those of the second approach. An explanation of this fact is that the modal approach has been restricted to only one mode of vibration. Although at resonance, the first mode possesses the main part of the energy of the system, the effects of the neglected modes can be perceptible on the sensitive behaviours as found in the chaotic state.

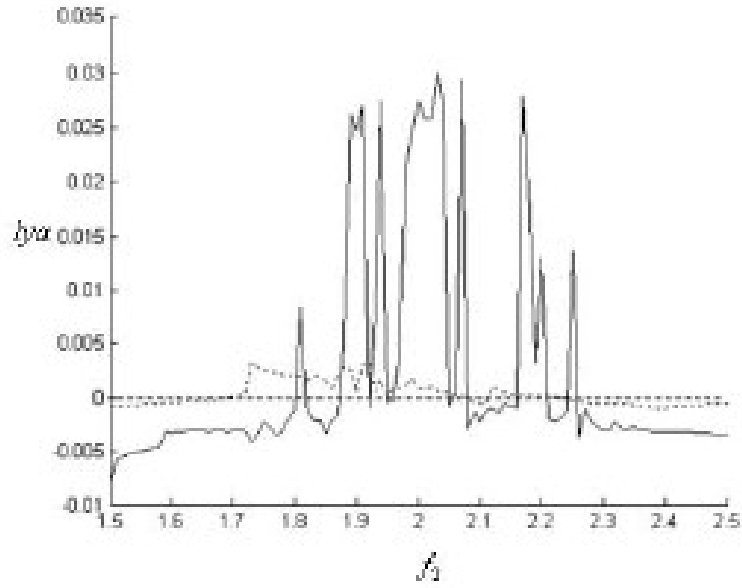


Figure 4: Variation of the Lyapunov exponent as function of the coupling coefficient f_2 from the modal approach (lines) and from the finite difference simulation (dash line) with

$$b = 0.1; a = \frac{1}{k_1^2}; w_{01} = w_0 = 1; \varepsilon_1 = 2.466; f_1 = 3.518; .$$

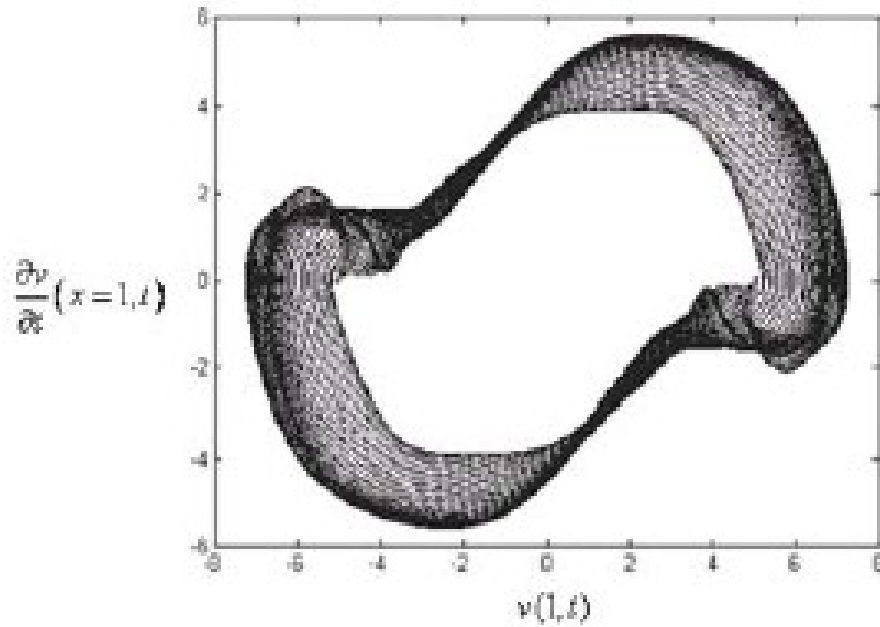


Figure 5a

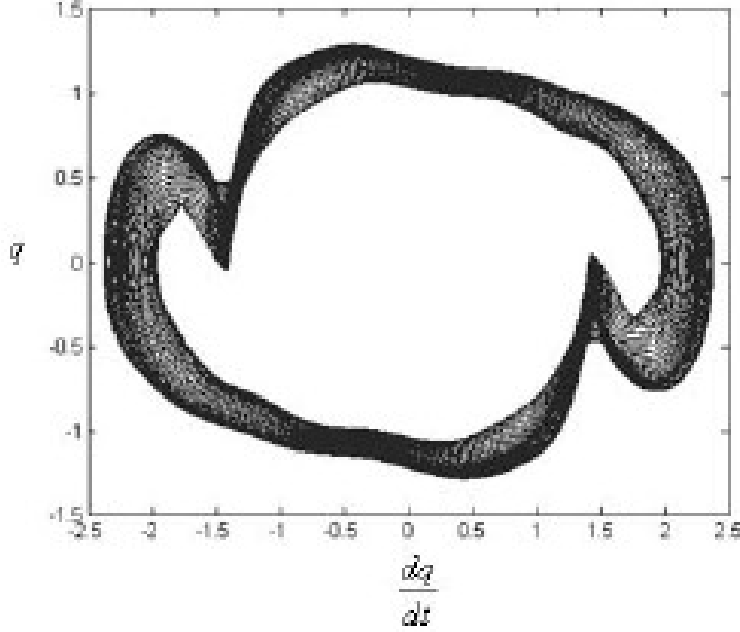


Figure 5b

Figure 5: Phase portrait of the mechanical part (a) and electric part (b) from the finite difference simulation with the parameters of Figure 5 and $f_2 = 2.2$.

The next section is devoted to the synchronization of the regular and chaotic states of two electromechanical devices.

5. SYNCHRONIZATION OF TWO SELF-SUSTAINED ELECTROMECHANICAL SYSTEMS WITH FLEXIBLE ARM

5.1 Model and Equations of Motion

In this section, we derive the characteristics of the unidirectional synchronization of two self-sustained electromechanical devices with flexible arm. The master system is described by the components q and v , while the slave system has the corresponding components p and u . The enslavement is carried out by an electric device consisting of operational amplifiers (see Figure 7). The equations of the slave are

$$\frac{d^2 p}{dt^2} - \varepsilon_1 \left(1 - \left(\frac{dp}{dt} \right)^2 \right) \frac{dp}{dt} + w_0^2 p + bp^3 + f_2 \frac{\partial u}{\partial t} \delta(x - x_1) + K(p - q)H(t - T_0) = 0 \quad (33)$$

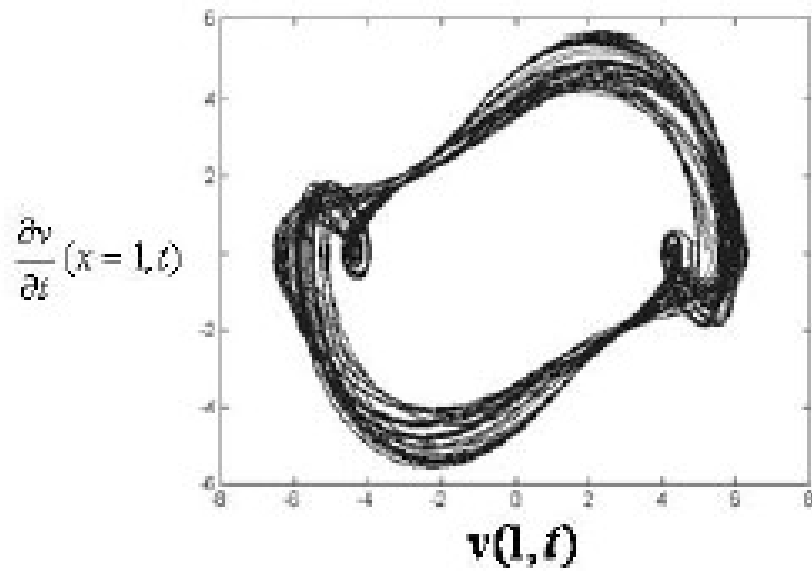


Figure 6a

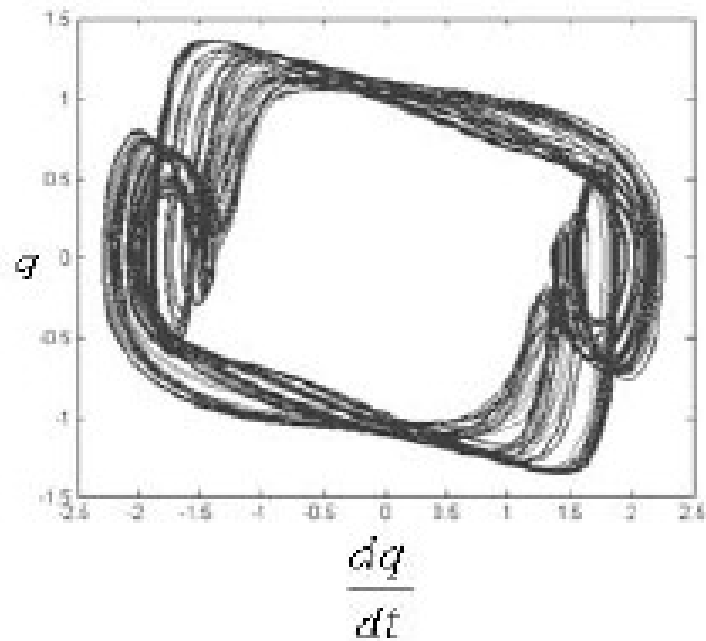


Figure 6b

Figure 6: Phase portrait of the mechanical part (a) and electric part (b) from modal approach with the parameters of Figure 5 and $f_2 = 2.2$.

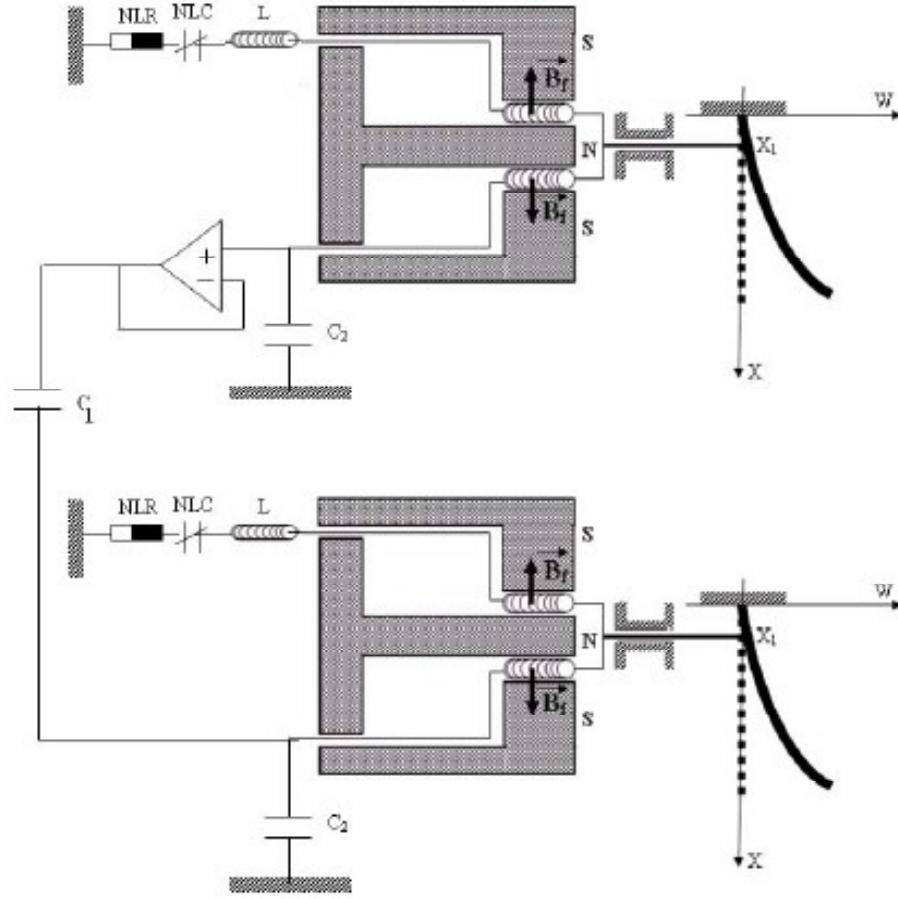


Figure 7: The Master-slave electromechanical devices

$$\frac{\partial^2 u}{\partial t^2} + \varepsilon_2 \frac{\partial u}{\partial t} + a \frac{\partial^4 u}{\partial x^4} - f_1 \frac{dp}{dt} \delta(x - x_1) = 0 \quad (34)$$

In the modal approach, they transform themselves to

$$\frac{\partial^2 p}{dt^2} - \varepsilon_1 \left(1 - \left(\frac{dp}{dt} \right)^2 \right) \frac{dp}{dt} + w_0^2 p + bp^3 + f_{21} \frac{d\Upsilon_1}{dt} + K(p - q)H(t - T_0) = 0 \quad (35)$$

$$\frac{d^2 \Upsilon_1}{dt^2} + \varepsilon_2 \frac{d\Upsilon_1}{dt} + w_0^2 \Upsilon_1 - f_{11} \frac{dp}{dt} = 0 \quad (36)$$

where $K = \frac{C_1}{C_2(C_1+C_2)L\omega_1}$ (with $C_0 \gg C_2$), is the dimensionless feedback coupling coefficient or strength, $H(x)$ the Heaviside function defined as $H(x) = 0$ for $x = 1$ for $x > 0$, and T_0 the onset time of synchronization.

5.2 The Formalism for Optimal Synchronization

When the synchronization process is launched, the slave configuration changes and one would like to determine the range of K for the synchronization to be achieved, and for the dynamics of the slave to remain stable. To carry out such an investigation, let us introduce the following variables $\zeta = p - q$ and $z = u - v$ which measure the nearness of the slave to the master. Introducing these variables in equation (35) and (36) and taking $z(x, t) = \eta_1(t) \phi_1(x)$, we obtain that ζ and η_1 satisfy the variational equations

$$\frac{d^2\zeta}{dt^2} - \varepsilon_1 \left(1 - \left(\frac{dq}{dt}\right)^2\right) \frac{d\zeta}{dt} + \Omega^2 \zeta + f_{21} \frac{d\eta_1}{dt} = 0 \quad (37)$$

$$\frac{d^2\eta_1}{dt^2} + \varepsilon_2 \frac{d\eta_1}{dt} + w_0^2 \eta_1 - f_{11} \frac{d\zeta}{dt} = 0 \quad (38)$$

where $\Omega^2 = w_0^2 + 3bq^2 + K$

The synchronization process is achieved when ζ and z go to zero as t increases or, practically, are less than a given precision. The behaviour of the slave depends on K and the form of the master. Assuming that ε_1 is small, the master variables take the form

$$q = A \cos(\omega_0 t - \varphi_1) \quad (39)$$

$$y_1 = B \cos(\omega_{01} t - \varphi_2) \quad (40)$$

where the amplitudes A and B depend on the system parameters as described by equations (26) and (27). With this form of the master, equations (37) and (38) takes the form

$$\frac{d^2\zeta}{dt^2} + F_1(t) \frac{d\zeta}{dt} + G_1(t) \zeta + f_{21} \frac{d\eta_1}{dt} = 0 \quad (41)$$

$$\frac{d^2\eta_1}{dt^2} + F_2(t) \frac{d\eta_1}{dt} + G_2(t) \eta_1 - f_{11} \frac{d\zeta}{dt} = 0 \quad (42)$$

with $F_1(t) = \lambda_0 - \frac{3}{2} A^2 \omega_0^2 \varepsilon_1 \cos(2\xi)$, $G_1(t) = \Omega^2$, $\lambda_0 = \varepsilon_1 \left(-1 + \frac{3}{2} A^2 \omega_0^2\right)$, $F_2(t) = \varepsilon_2$, $G_2(t) = \omega_{01}^2$,
 $\xi = \omega_0 t - \gamma_1$.

Setting the following transformations

$$\zeta = U \exp\left(-\frac{1}{2} \int F_1(t) dt\right) \quad (43)$$

$$\eta_1 = V \exp\left(-\frac{1}{2} \int F_2(t) dt\right) \quad (44)$$

we rewrite equations (41) and (42) in the standard form

$$\frac{d^2 U}{dt^2} + F(t)U + f_{21} \left(\frac{dV}{dt} - G_2(t)V \right) \exp(\psi) = 0 \quad (45)$$

$$\frac{d^2 V}{dt^2} + G(t)V + \left(R(t)U - f_{11} \frac{dU}{dt} \right) \exp(-\psi) = 0 \quad (46)$$

with

$$F(t) = \delta_{11} + 2\epsilon \sin(2\xi) + 2\epsilon_{12} \cos(2\xi) + 2\epsilon_{13} \cos(4\xi), \quad G(t) = \delta_{21},$$

$$R(t) = \delta_{22} + 2\epsilon_{21} \cos(2\xi), \quad \psi = -\frac{1}{2}(\epsilon_2 - \lambda_0)t + \frac{3}{8}A^2 w \epsilon_1 \sin(2\xi),$$

$$\delta_{11} = \Omega^2 - \frac{\lambda_0^2}{4} - \frac{9}{32}A^4 w^4 \epsilon_1, \quad \epsilon_{11} = -\frac{3}{4}A^4 w^3 \epsilon_1, \quad \epsilon_{12} = \frac{3}{4}bA^2 + \frac{3}{8}A^2 w^2 \lambda_0 \epsilon_1,$$

$$\epsilon_{13} = -\frac{9}{64}A^4 w^4 \epsilon_1^2, \quad \delta_{22} = \frac{\lambda_0 f_{11}}{2}, \quad \epsilon_{21} = -\frac{3}{8}A^2 w^2 \epsilon_1 f_{11}, \quad \delta_{21} = w_{01}^2 - \frac{\epsilon_2^2}{4}.$$

Equations (45) and (46) are two coupled Hill's equations. According to the Floquet theory [12,13], the solutions are

$$U = \alpha(t) \exp(\theta_1(t)) = \sum_{n=-\infty}^{n=+\infty} \alpha_n \exp(a_n t) \quad (47)$$

$$V = \beta(t) \exp(\theta_2(t)) = \sum_{n=-\infty}^{n=+\infty} \beta_n \exp(b_n t) \quad (48)$$

where $a_n = \theta_1 + 2Jn\omega_0$, $b_n = \theta_2 + 2Jn\omega_0$ ($J^2 = -1$). The function $\alpha(t) = \alpha(t + \pi)$ and $\beta(t) =$

$\beta(t + \pi)$ are replaced by the Fourier series, with $\theta_1, \theta_2 \in C$ and $\alpha_n, \beta_n \in R$. Inserting equations (47) and (48) into equation (45) and (46) yields ($\forall n \in N$)

$$\sum_{n=-\infty}^{n=+\infty} e^{2Jn\omega_0} \left\{ \begin{array}{l} \alpha_n (a_n^2 + \delta_{11}) + \alpha_{n+1} (\epsilon_{11} + J \epsilon_{11}) e^{\psi_2} + \alpha_{n-1} (\epsilon_{12} - J \epsilon_{11}) e^{-\psi_1} + \\ \alpha_{n+2} \epsilon_{13} e^{-2\psi_1} + \alpha_{n-2} \epsilon_{13} e^{2\psi_2} + f_{21} \beta_n \left(b_n - \frac{\epsilon_2}{2} \right) e^v \end{array} \right\} = 0 \quad (49)$$

$$\sum_{n=-\infty}^{n=+\infty} e^{2Jn\omega_0} \left\{ \alpha_n (-f_{11} a_n + \delta_{22}) e^{-v} + \alpha_{n+1} \epsilon_{21} e^{\psi_2 - v} + \alpha_{n-1} \epsilon_{21} e^{-\psi_1 - v} + \beta_n (b_n^2 + \delta_{21}) \right\} = 0 \quad (50)$$

Equating each of the coefficients of the exponential functions to zero one obtains the following infinite set (S) of linear, algebraic, homogeneous equations for the α_n and β_n

$$(S) \left\{ \begin{array}{l} \alpha_n (a_n^2 + \delta_{11}) + \alpha_{n+1} (\epsilon_{12} + J \epsilon_{11}) e^{\psi_2} + \alpha_{n-1} (\epsilon_{12} - J \epsilon_{11}) e^{-\psi_1} + \\ \alpha_{n+2} \epsilon_{13} e^{-2\psi_1} + \alpha_{n-2} \epsilon_{13} e^{2\psi_2} + f_{21} \beta_n \left(b_n - \frac{\epsilon_2}{2} \right) e^\psi = 0 \\ \alpha_n (-f_{11} a_n + \delta_{22}) e^{-\psi} + \alpha_{n+1} \epsilon_{21} e^{\psi_2 - \psi} + \alpha_{n-1} \epsilon_{21} e^{-\psi_2 - \psi} + \beta_n (b_n^2 + \delta_{21}) = 0 \end{array} \right. \quad (51)$$

where $v = \left(\theta_2 - \frac{\epsilon_2}{2} \right) t - \left(\theta_1 - \frac{\lambda_0}{2} \right) t + \frac{3}{8} A^2 \omega_0 \epsilon_1 \sin(2\xi)$, $\psi_1 = 2J\gamma_1 + \theta_1 t$, $\psi_2 = 2J\gamma_1 + \theta_2$

Applying the consideration of Ref. [5], we find that the boundary, that separates the stability from the instability domains, is given by

$$\det(S) = 0 \quad (52)$$

Here we limit the calculation to the sixth order Hill's determinant of the algebraic system (S). Since, we have

$$\zeta = \exp \left\{ \left(\theta_1 - \frac{\lambda_0}{2} \right) t - \frac{3}{8} \epsilon_1 w A^2 \sin(2\xi) \right\} \alpha(t) \quad (53)$$

$$\eta_1 = \exp \left\{ \left(\theta_2 - \frac{\epsilon_2}{2} \right) t \right\} \beta(t) \quad (54)$$

the Floquet theory states that the transition from stability to instability domains (or the the reverse) occurs only in the two following conditions:

- π - periodic transitions at $\theta_1 = \theta_1^1 = \frac{\lambda_0}{2}$ and $\theta_2 = \theta_2^1 = \frac{\epsilon_2}{2}$

- 2π - periodic transitions at $\theta_1 = \theta_1^2 = \frac{\lambda_0}{2} + J$ and $\theta_2 = \theta_2^2 = \frac{\epsilon_2}{2} + J$.

Thus replacing θ_k by θ_k^k ($k = 1, 2$) in equation (52), we obtain an equation which helps us to determine the range of K in which the synchronization process is stable.

5.3 Synchronization of the Oscillatory Dynamics

In this sub-section we consider the master and the slave systems with a periodic behaviour and compare the results of numerical simulation of equations (33) and (34) and equations (35) and (36) to that of the above analytical treatment. The amplitude $A = 0.31$ is obtained from equations (26) and (27) with $\epsilon_2 = 0.01$ while the frequency ω_0 is set equal to ω_{01} (at the resonance). From equation (52), the stability is achieved for $K \in]-11.36; 0] \cup]0; +\infty]$ with the parameters of Figure 2. For the numerical simulation of equations (33) and (34) along with equations (9) and (10) and equations (16) and (17) of the master, we use the initial conditions $\left(q, \frac{dq}{dt}, v, \frac{\partial v}{\partial t}\right) = (5.0, 5.0, 0.0, 0.0)$ for the master and $\left(p, \frac{dp}{dt}, u, \frac{\partial u}{\partial t}\right) = (4.0, 4.0, 0.0, 0.0)$ for the slave. We obtain that the synchronization domain is $K \in]-12.4; 0] \cup]0; +\infty]$ from the modal approach (ordinary differential equations) and $K \in]-12.6; 0] \cup]0; +\infty]$ from the direct numerical simulation of the partial differential equations. We take $T_0 = 800$ and assume that the synchronization is achieved when $|q - p| < h_0, \forall t > T_0$ with $h_0 = 10^{-10}$. Figure 8 shows the synchronization time T_s versus K . The agreement between the two approaches and the analytical investigation is quite acceptable. The singularity at $K = -0.7$ can be the signature of parametric resonances.

5.4 Case of Chaotic States

Hereafter the master and slave systems are in the chaotic state, we proceed to numerical simulation of equations (33) and (34) and (35) and (36) to determine the range of K for which the synchronization is achieved. The criterion of numerical synchronization is that used for the regular state. The initial conditions are $\left(q, \frac{dq}{dt}, v, \frac{\partial v}{\partial t}\right) = (3.5, 3.2, 0.0, 0.0)$ for the master and $\left(p, \frac{dp}{dt}, u, \frac{\partial u}{\partial t}\right) = (4.0, 4.0, 0.0, 0.0)$ for the slave. We find that the synchronization is achieved for $K \in]1.5; 3.7] \cup]3.8; 4.2] \cup]4.2; 8] \cup]11; 15]$, while the finite differences simulation gives the synchronization for $K \in]0.4; 15]$. The synchronization time T_s is plotted versus K and the results are reported in Figure 9 for the two approaches. The differences between the modal approach and the finite difference simulation is very important

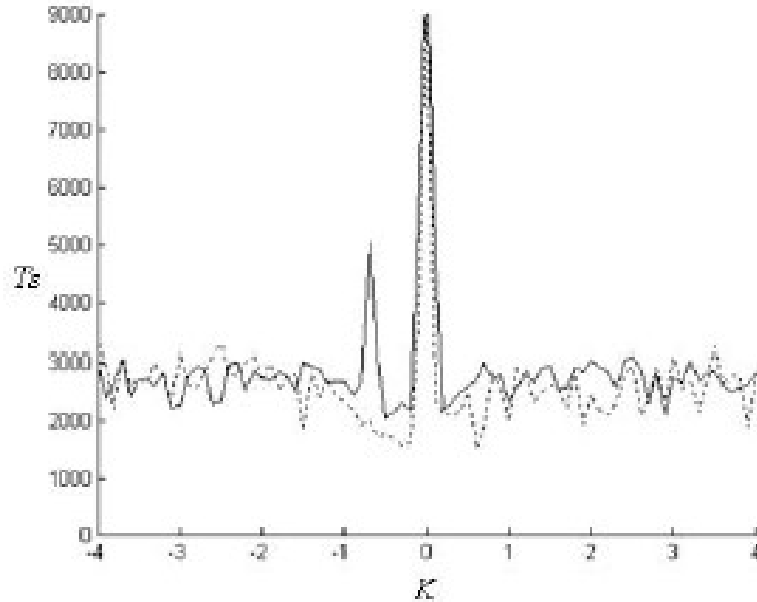


Figure 8: Synchronization time T_s versus K with the parameter of Figure 2 and $\epsilon_2 = 0.01$ from the finite difference simulation (dash line) and the modal approach (line)

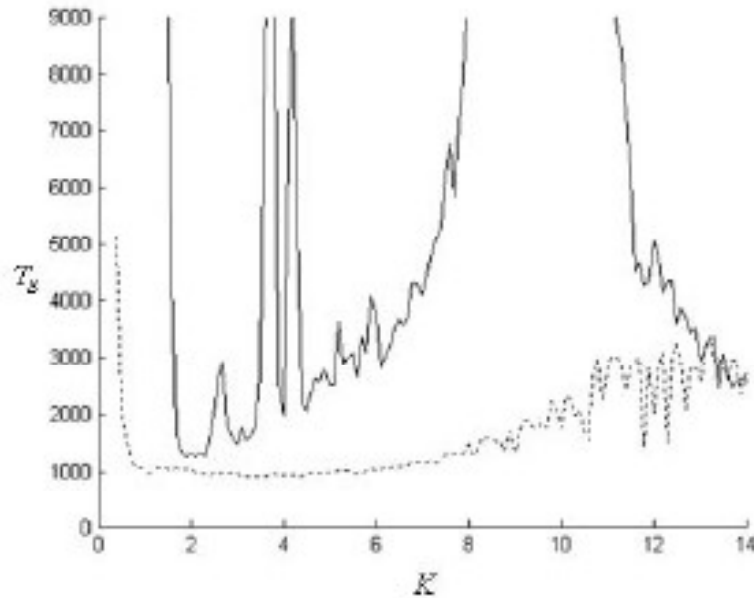


Figure 9: Synchronization time T_s versus K with the parameter of figure 5 from the finite difference simulation (dash line) and the modal approach (line) in the chaotic regime

if compared to what is observed in the case of oscillatory behaviour. This is understandable since the harmonic oscillatory approximation (equations (39) and (40) used for the formulism is invalid here. Indeed, it can not approximate the time behaviour of the chaotic state. Figures 10 and 11 show respectively the deviations between the slave and the master in the case of synchronization and in the case where the synchronization process has failed.

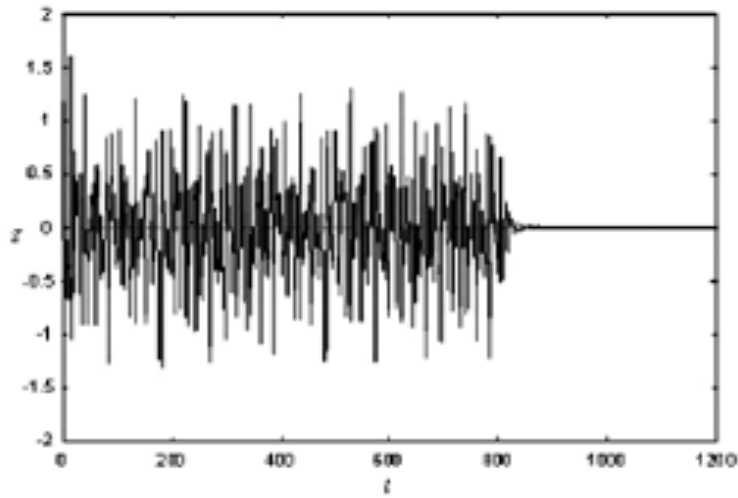


Figure 10a

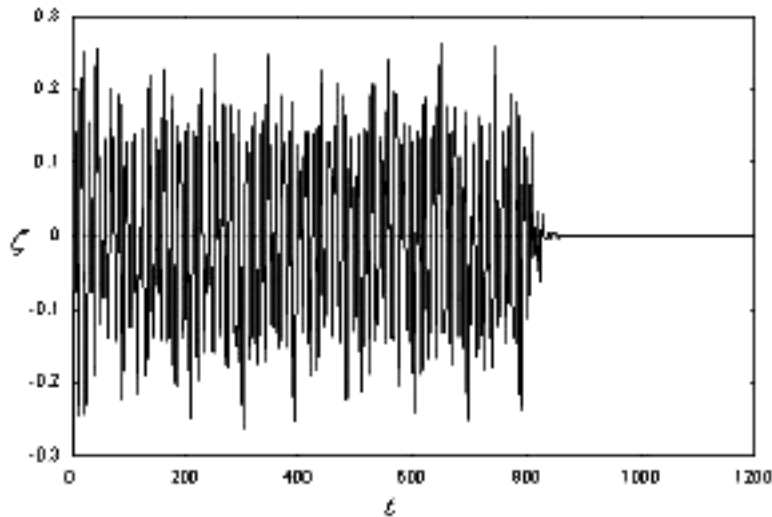


Figure 10b

Figure 10: Time history of the deviations z (a) and ζ (b) with the parameters of Figure 5 and $K = 3$ from finite difference simulation: case of synchronization failure.

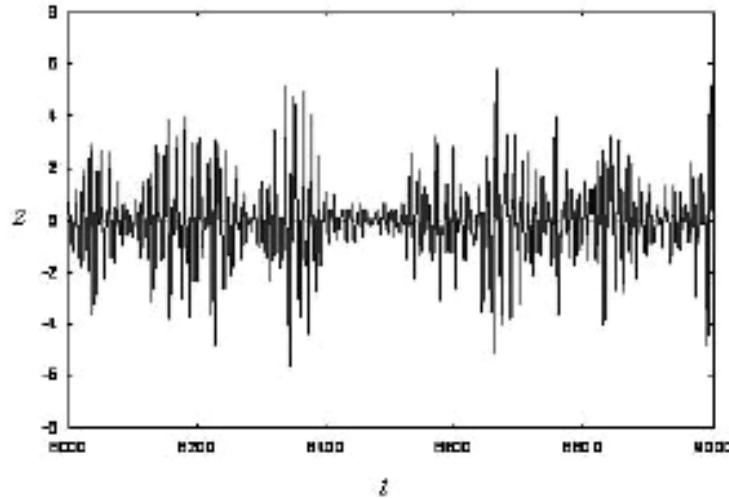


Figure 11a

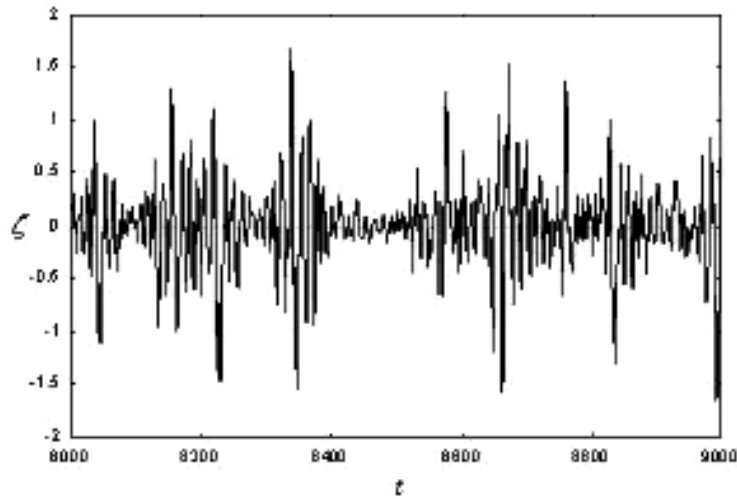


Figure 11b

Figure 11: Time history of the deviations z (a) and ζ (b) with the parameters of Figure 5 and $K = -1$ from the finite difference simulation: case of synchronization.

6. CONCLUSION

This paper has dealt with the dynamics, chaos and synchronization of self-sustained electromechanical systems with flexible arm consisting of a Rayleigh-Duffing oscillator coupled magnetically to a flexible beam. The averaging method has been used to determine the amplitudes of the oscillatory behaviour. The Lyapunov exponent helps us to study the chaotic behaviour and typical chaotic phase portraits were reported. For the synchronization

process, the analytical investigation has been based on the properties of the Hill equation which describes the deviation between the slave and the master devices. The analytical results have been compared to those of the semi-analytical studies as well as to those of a direct numerical simulation of the partial differential equations. The next step following this study is to carry out experimental investigations where the effects of parameters mismatch is unavoidable.

REFERENCES

- [1] Chedjou JC, Wofo P, Domngang S. Shilnikov, chaos and dynamics of a self-sustained electromechanical transducer. *ASME Journal of Vibration and Acoustics* 2001; 123: 170-174.
- [2] Jerrelind J, Stensson A. Nonlinear dynamics of parts in engineering systems. *Chaos, Solitons and Fractals* 2000; 11: 2413-2428.
- [3] Chembo Kouomou Y, Wofo P. Triple resonant states and chaos control in an electrostatic transducer with two outputs. *J. Sound and Vibration* 2004; 270: 75-92.
- [4] Luo ACJ, Wang FY. Nonlinear dynamics of a micro-electromechanical system with time-varying capacitors. *ASME Journal of vibration and Acoustics* 2004; 126: 77-83.
- [5] Yamapi R, Wofo P. Dynamics and synchronization of self-sustained electromechanical devices. *J. Sound and Vibration* 2005; 285: 1151-1170.
- [6] Yamapi R, Wofo P. Synchronized states in a ring of four mutually coupled self-sustained electromechanical devices. *Commun. Nonlinear Science and Numerical Simulation* 2006; 11: 186-202.
- [7] Raskin JP, Brown AR, Khuri-Yakub BT, Rebeiz GM. A novel parameter MEMS amplifier. *J. Microelectromechanical Systems* 2000; 9: 528-537.
- [8] Skkasoglu A, Vavriv D. Interaction of low and high-frequency oscillations in a nonlinear RLC circuit. *IEEE Trans. on Circuit and Systems-I* 1994; 41: 669-672.
- [9] Hasler MJ. Electrical circuit with chaotic behaviour. *Proceedings of the IEEE* 1987; 75: 1009-1021.
- [10] King GP, Gaito ST. Bistable Chaos I: Unfolding the cusp. *Phys. Rev. A* 1992; 46: 3092-3099.
- [11] Timoshenko S and Gere JM. *Theory of Elastic Stability*. 2nd ed. New York: McGraw-Hill; 1961.
- [12] Nayfeh AH, Mook DT. *Nonlinear Oscillations*. New York: Wiley; 1970.
- [13] Hayashi C. *Nonlinear Oscillations in Physical Systems*. New York: McGraw-Hill; 1964.

C.A. Kitio Kwiimy & P. Wofo

Laboratory of Nonlinear Modeling and Simulation in
Engineering and Biological Physics
University of Yaounde I, Box 812, Yaounde, Cameroon.
E-mail: pwofo@uycde.uninet.cm